Simulation of continuously regenerating trap with catalyzed DPF

Kazuhiro Yamamoto, Tatsuya Sakai

Department of Mechanical Science and Engineering, Nagoya University

Furo-cho, Chikusa-ku, Nagoya, Aichi 464-8603, JAPAN

kazuhiro@mech.nagoya-u.ac.jp

Keywords: Catalyst; DPF; Continuously regenerating trap; Diesel exhaust; Computed Tomography

ABSTRACT

For reduction of particulate matter (PM) including soot in diesel exhaust gas, a diesel particulate filter (DPF) has been developed. However, it would be plugged with PM to cause an increase of filter backpressure. If the backpressure is too high, the fuel consumption rate unexpectedly increases and the engine output may decrease. Then, the filter must be regenerated by oxidizing PM. The system where PM is trapped and oxidized simultaneously is called a continuously regenerating DPF. A catalyst such as platinum is used for the reduction of PM oxidation temperature. Since platinum is a precious and rare metal, the amount of catalyst must be suppressed. In this study, we simulated the continuously regenerating trap system with catalyzed DPF by a lattice Boltzmann method (LBM). For the soot oxidation rate with catalysts, reaction parameters such as activation energy were evaluated by an engine test bench. In the simulation, five cases with different catalyst-coating were considered. Based on the filter backpressure, the coating area for the reduction of catalysts was discussed.

1. Introduction

The reduction of carbon dioxide (CO_2) emissions is essential for inhibiting global warming. The use of fuel-efficient diesel vehicles is one strategy for reducing CO_2 emissions [1], and the number of diesel vehicles has been increasing, particularly in Europe. However, diesel vehicles emit nitrogen oxides (NO_x) and particulate matter (PM) in the form of soot, which cause air pollution. Measures to reduce nanoparticulate soot emission are particularly important, because nanoparticles pose particular health risks for diseases such as cancers [2-4]. Therefore, regulations for the control of automobile exhaust gas emissions are being strengthened year after year [5]. Meeting these regulations requires not only improving fuel efficiency but also improving the exhaust gas after-treatment system. Diesel particulate filters (DPFs), which collect PM, are widely used for exhaust gas treatment [6-8].

Figure 1 shows a schematic of DPF. Upper figure shows PM trap inside porous filter wall. A typical DPF is made of porous ceramics with a honeycomb structure, and has the alternate closure of the inlets and outlets of its many channel holes. The mechanism for PM trap is simple: when the exhaust gas passes through the cell walls (the filter's sidewalls), which separate cells at inlet and outlet sides of the filter, PM contained in the gas is deposited within the filter wall. However, as PM is continuously collected, the filter eventually clogs, and the exhaust pressure (filter backpressure) increases [9,10]. Consequently, the fuel consumption rate

unexpectedly increases and the engine output may decrease. These disadvantages can be avoided by using a continuously regenerating DPF [4,5], which collects PM and simultaneously oxidizes it. To oxidize the PM at low temperature, DPFs with precious metal catalysts such as platinum are in practical use [11,12].

However, catalysts made of precious and rare metals are very expensive, so the amount of catalysts must be reduced to make these filters cost-effective. This requires an understanding of the phenomena occurring within the thin sidewalls of DPFs. Therefore, processes that would allow visualization of these phenomena and examination of the effects of catalysts would be valuable, but these are very difficult in experiments [13]. Our research group has been investigating the phenomena occurring within DPFs by conducting numerical simulations using a lattice Boltzmann method (LBM) [14-17], which is effective for analyzing a porous media flow [18]. The present study numerically simulated a continuously regenerating DPF for the reduction of the catalyst amount required to support its operation.

Fig.1

2. Numerical analysis

2.1. Lattice Boltzmann method

Firstly, the numerical approach for exhaust gas flow with soot oxidation is explained, followed by the soot deposition model described at the next section. The lattice Boltzmann method (LBM) was used in the simulation, which is a simplification of Boltzmann equation [18]. The LBM analyses the flow based on the movement and collision processes of artificial particles moving at lattice nodes. So far, many fluid simulations by LBM have been conducted, including the flow in DPF [13-17]. The model of D3Q15 using cubic lattices is usually used for 3D calculation [19].

As for the combustion simulation, we followed the same numerical scheme proposed in our previous study [13, 20]. The flow field was determined using the distribution function of pressure, *p*. The evolution equation and the equilibrium distribution function are expressed as follows:

$$F_{p,\alpha}(\vec{x}+\vec{e}_\alpha\delta_t, t+\delta_t) - F_{p,\alpha}(\vec{x},t) = -\frac{1}{\tau_p}[F_{p,\alpha}(\vec{x},t) - F^{eq}_{p,\alpha}(\vec{x},t)] \quad (1)$$

$$F^{(eq)}_{p,\alpha} = w_\alpha \left\{ p + p_0 \left[3\left(\frac{\vec{e}_\alpha \cdot \vec{u}}{c^2}\right) + \frac{9}{2}\left(\frac{\vec{e}_\alpha \cdot \vec{u}}{c^2}\right)^2 - \frac{3}{2}\left(\frac{\vec{u}}{c}\right)^2 \right] \right\} \quad (2)$$

where δ_t is the time step, τ is the relaxation time which controls the rate of approach to equilibrium, and $\vec{e}_\alpha$ (α

= 1 - 15) is the unit vector of D3Q15 model in lattice space. The constants in Eq. (2) are $w_{1\text{-}6}$=1/9, $w_{7\text{-}14}$=1/72, and w_{15}=2/9. The pressure, p, and the local velocity of $\vec{u}$ = (u, v, w) are obtained using the low Mach number approximation [20] as follows:

$$p = \sum_{\alpha} F_{p,\alpha} \qquad (3)$$

$$\vec{u} = \sum_{\alpha} \frac{F_{p,\alpha}}{P_{out}} \cdot \frac{T_0}{T} \vec{e}_{\alpha} \qquad (4)$$

where P_{out} represents atmospheric pressure. The kinematic viscosity of v in LBM is related with the relaxation time of τ, using the following formula:

$$\nu = \frac{2\tau_p - 1}{6} \frac{\delta_x^2}{\delta_t} \qquad (5)$$

Through the Chapman-Enskog procedure, the Navier-Stokes equations are derived from these equations [18]. In the calculation, all of the variables were set to be dimensionless, and the same dimensionless quantities

such as the Reynolds number (Re = $U_{in}W / \nu$) were used [20], where U_{in} is the inlet velocity of exhaust gas, and W is the width of numerical domain in **Fig. 3**.

Similar to the flow field, the scalar quantities of temperature and species concentrations were also determined by their distribution functions [13-17, 20]. The evolution equation and the equilibrium distribution function for the scalar quantities are expressed as follows:

$$F_{s,\alpha}(\vec{x}+\vec{e}_\alpha\delta_t, t+\delta_t) - F_{s,\alpha}(\vec{x},t) = -\frac{s}{\tau_s}[F_{s,\alpha}(\vec{x},t) - F_{s,\alpha}^{(eq)}(\vec{x},t)] + w_\alpha Q_s \qquad (6)$$

$$F_{s,\alpha}^{(eq)}(\vec{x},t) = w_\alpha s\left\{1+3\left(\frac{\vec{e}_\alpha\cdot\vec{u}}{c^2}\right)+\frac{9}{2}\left(\frac{\vec{e}_\alpha\cdot\vec{u}}{c^2}\right)^2-\frac{3}{2}\left(\frac{\vec{u}}{c}\right)^2\right\} \qquad s = T, Y_i \qquad (7)$$

where s is the value of temperature and mass fraction of species i, and Q_s represents the source term due to the chemical reaction in the soot oxidation process. The procedure to evaluate the soot oxidation rate in catalyzed DPF will be explained later. An overall one-step reaction of $C + O_2 \rightarrow CO_2$ was used [13, 21]. For relaxation time of τ_s, which is required for calculating the concentration and temperature fields, the same value as that of τ_p in Eq. (5) was used. The temperature and the mass fraction of species i (mass fraction) are obtained as

follows:

$$T = \sum_{\alpha} F_{T,\alpha} \qquad (8)$$

$$Y_i = \sum_{\alpha} F_{Y_i,\alpha} \qquad (9)$$

2.2. Soot deposition model

In this section, a soot deposition model is explained. Generally, the soot has complex geometry of nanoparticles [2, 22, 23]. Since the size of diesel soot has a nano-scale, it is difficult to realize the deposition phenomenon of soot particles precisely. Then, the soot deposition is described by the modified particle deposition model [24]. Different from Lagrangian approach through the equation of motion, individual particles were not considered. Instead, the soot concentration was monitored. The mass fraction of deposited soot is given by

$$Y_{C,s}(\vec{x},\ t+\delta_t) = \sum_{\alpha} F_{C,\alpha}(\vec{x},\ t)\cdot P_D + Y_{C,s}(\vec{x},\ t) \qquad (10)$$

where $Y_{C,s}$ is the mass fraction of deposited soot of solid phase, and P_D is the soot deposition probability,

which controls the amount of soot attached to the filter substrate. If P_D is unity, soot is thoroughly deposited on the filter without reflection. Else, a part of soot is bounced back and transported downstream. As the soot deposition is continued, the soot mass fraction sometime becomes unity. When this limit is reached, the solid site is piled up, and the deposited soot region is treated as non-slip wall, which implies a change of boundary condition for fluid. In the simulation, we adopted $P_D = 0.002$, which is the value determined in experiments [16,17].

2.3. Numerical domain

Here, we describe the numerical domain in the simulation. **Figure 2** shows an image of the filter obtained by a three-dimensional X-ray CT measurement. The image area was 0.66 mm (y) × 0.66 mm (z), and the spatial resolution was 1.15 μm/pix. **Figure 3** shows the filter and the coordinate system used in the simulation. The direction of exhaust gas flowing into the filter (the direction perpendicular to the side walls) is x, and the directions perpendicular to the flow direction are y and z. The inner structure of the filter was analyzed in the three-dimensional coordinate, and the part of the CT data was used in the simulation, which is called a tomography-assisted simulation [13-17]. The filter size of 250 μm (x) × 46 μm (y) × 46 μm (z) was

placed on the center of the numerical domain, and entrance zones of 50 μm were set before and after the filter. Therefore, the entire size of the numerical domain was 350 μm (x) × 46 μm (y) × 46 μm (z), and the number of lattices was 305 (x) × 41 (y) × 41 (z).

Fig.2

The boundary conditions were as follows: the slip boundary was applied as a symmetrical boundary to the four sidewalls (top, bottom, right, and left) in **Fig. 3**. The outlet was set as a free outflow boundary with a constant pressure (atmospheric pressure). A non-slip boundary with a zero velocity was adopted for the filter substrate and soot layer surfaces. The temperature at the inlet was 400 ℃, and the exhaust gas containing soot with a mass fraction of 0.01 was flowed into the filter at a velocity of 1.0 cm/s. The oxygen concentration (volume concentration) of the exhaust gas was 10% (mass fraction of 0.113 [15]). As already mentioned, the soot deposition probability was 0.002. The gas phase temperature was increased by the oxidation of deposited soot on the filter substrate. The filter substrate was set as thermal insulation [25].

To investigate the effect of catalysts, the amount of catalyst was changed by using different areas of the catalyst. The catalyst was uniformly adhered to the surface of the filter substrate. Table 1 shows five cases with different catalyst-coating. In case 1, no catalysts were used. In case 2, the entire filter substrate was covered by the catalyst. In case 3A, 1/3 of the entire filter substrate at the upstream side was covered by the

catalyst. On the other hand, in cases 3B and 3C, 1/3 of the entire filter substrate at the middle or the downstream was covered by the catalyst.

Fig.3

Table 1

3. Results and discussion

3.1. Soot oxidation rate with catalyst

First of all, the soot oxidation rate was evaluated by the engine test bench [10, 15], equipped with the catalyzed DPF. **Table 2** shows the engine specifications. Here, the experimental procedure was explained. Initially, some amount of diesel soot was trapped inside DPF. Then, the temperature was increased for the filter regeneration. By measuring the emissions of CO and CO_2, the mass of oxidized soot was calculated to obtain the reaction constants such as activation energy. The soot oxidation rate was assumed as the first-order reaction of the soot concentration (soot mass) with the following Arrhenius type equation [15]:

Table 2

$$-\frac{dm}{dt} = km, \qquad k = A\exp\left(-\frac{E}{RT}\right) \qquad (11)$$

where m represents the mass of unreacted soot inside DPF, k represents a reaction rate constant, A represents a pre-exponential factor, E represents activation energy, and R represents the gas constant. Based on the Arrhenius plots, the frequency factor was 5.92×10^9 1/s, and activation energy was 184 kJ/mol.

It is well-known that the catalyst reduces the activation energy and promotes the chemical reaction. To make clear the effect of catalyst, the reaction constants with and without catalyst are compared. The reaction rate without catalyst was the value in our previous experiments [15]. The obtained reaction rate constant, k, is shown in **Fig. 4**. The value with catalyst is much larger than that without catalyst. It is found that, above 700 K, the reaction rate constant is largely increased. That is, the soot oxidation is much promoted in this temperature range.

Fig.4

3.2. Effect of catalyst

Here, the effect of the catalyst was examined. **Figure 5** shows the soot deposition regions in cases 1 and 2, obtained at $t = 120$ s. Initially, the filter is clean, and the exhaust gas with soot is flowed into the filter at $t = 0$. The black region indicates the soot deposition layer on the surface of the filter substrate, where the mass fraction of deposited soot, $Y_{c,s}$, is over 0.001. In this figure, 2D profile in xy plane at the center ($z = 23$ μm)

shows the distribution of soot mass fraction in gas phase. It is found that the soot deposition widely occurs inside DPF in case 1. However, in case 2, less soot layer is observed. Correspondingly, when the catalyst is adhered to the surface of the filter substrate, the soot oxidation is promoted. Resultantly, even if the soot in gas phase is deposited on the surface of the filter substrate, most of deposited soot is instantly oxidized with catalyst. This situation is ideal to realize the continuously regenerating DPF.

Fig.5

To reveal the time-variation of soot deposition region, results in cases 1 and 2 are compared. The soot deposition regions in cases 1 and 2 are shown in **Figs. 6 and 7**, respectively. These are 2D profiles in *xy* plane at t = 40, 80, and 120 s. Since there are no catalysts in case 1, the soot oxidization seldom occurs. Then, as seen in **Fig. 6**, the amount of soot deposited onto the filter substrate is increased with time. As the amount of deposited soot is increased, the soot layer is thickened especially at the upstream side of the filter. Resultantly, most of pores are clogged. However, as seen in **Fig. 7**, the amount of deposited soot is not increased much, because the deposited soot is instantly oxidized by the catalyst. In this case, the filter clogging can be avoided.

Fig.6

Fig.7

For further study, the combustion field is examined. Results in cases 1 and 2 are then compared. **Figures 8 and 9** show the results obtained at t = 120 s. These profiles are the mass fraction of soot in the gas phase ($Y_{c,g}$), the reaction rate (W_c), and the temperature (T), which are obtained in the *xy* plane at the center of the

numerical domain. It is noted that the maximum temperatures of Figs. 8c (case 1) and 9c (case 2) are 400.19 and 692.63 ºC, respectively. As seen in **Fig. 8a**, even in case 1, the soot concentration in the gaseous phase is decreased inside the filter. However, comparing to **Fig. 9b**, the soot oxidation rate in **Fig. 8b** is very small. Therefore, the reduction of soot concentration in gas phase is due to the soot deposition. This could be supported by the temperature change in **Fig. 8c**, where there is almost no temperature rise, because the initial temperature of the exhaust gas is 400 ºC. On the other hand, as seen in **Fig. 9c**, the temperature is increased by 292.63 ºC, which is surely due to soot oxidation on the catalysts. As a result, the soot layer in **Fig. 7** is not expanded, and the continuous regeneration could be realized.

Fig.8

Fig.9

The temporal changes in the amount of deposited soot and the filter backpressure (the difference in the pressure before and after the filter) were then investigated. **Figure 10a** shows the temporal changes in the soot amount in cases 1 and 2. **Figure 10b** shows the temporal changes in the filter backpressure. Here, the soot amount was expressed by the average soot density, which was the amount of soot deposited inside the filter divided by the entire filter volume. As shown in **Fig. 10a**, the amount of deposited soot in case 1 is increased, almost proportional to the time. In case 2, the amount of deposited soot is saturated. Thus, it is expected that amounts of deposited soot and oxidized soot are balanced. Resultantly, as seen in **Fig. 10b**, the filter

backpressure in case 2 is almost constant after t = 10 s. On the other hand, in case 1, since the amount of deposited soot is continuously increased, the filter backpressure is also kept rising. Fig.10

3.3. Catalyst support quantity

Finally, the amount of catalysts was changed to collect some information for the reduction of catalysts, by comparing cases 2 and 3. **Figure 11** shows the distributions of the soot deposition region in cases 3A, 3B, and 3C, which are the *xy* sections at the center of the calculation domain at t = 120 s. Interestingly, less soot layer is present at the upstream side of the filter in case 3A, but more soot is deposited in the downstream side. As shown in table 1, the catalyst is adhered only in the 1/3 upstream region. Then, as seen in case 2, the deposited soot in this area is instantly oxidized by the catalyst, and the growth of the deposited soot layer is prevented. Similarly, at the middle region in case 3B and the downstream region in case 3C, less soot layer is observed. Fig.11

Next, by comparing cases 3A, 3B, 3C, the effect of coating area is investigated. **Figure 12** shows the temporal change in the amount of deposited soot. The result in case 2 is also shown. Among three cases of 3A, 3B, 3C, the amount of deposited soot in case 3A is the smallest, where 1/3 of the filter substrate at the

upstream side was covered by the catalyst, and is the largest in case 3C where 1/3 of the filter substrate at the downstream side was covered by the catalyst. In other words, the catalyst coating at the upstream side is more effective. This could be due to the fact that more soot accumulation occurs at the upstream area of the filter (see **Fig. 5b**).

The amount of deposited soot is well related with the filter backpressure. **Figure 12b** shows the change in the filter backpressure in cases 2, 3A, 3B, and 3C. By comparing **Fig. 12a**, the backpressure gradually increases as the amount of soot deposited onto the filter surface is increased. However, no increase in the backpressure is seen in case 2. By comparing three cases of 3A, 3B, 3C, the increase of filter backpressure in 3A is the smallest. Moreover, the value of the filter backpressure in case 3A was almost equal to that in case 2.

In summary, when a part of the filter substrate was covered by the catalyst, the soot oxidation is promoted, and consequently, the amount of deposited soot inside the filter is reduced. When the catalyst was adhered in the 1/3 upstream region of the entire filter substrate, an increase in the filter backpressure is efficiently inhibited, suggesting that the catalyst coating at the upstream side is more effective. This information is very useful for the reduction of the catalysts.

Fig.12

4. Conclusions

The present study numerically simulated the continuously regenerating DPF, taking into consideration the deposition and oxidation of soot. In particular, we focused on the changes in the soot deposition and filter backpressure at different amount of catalysts. The results are summarized as follows:

1. When no catalysts are used, very little soot is oxidized in the gas phase, but is deposited onto the filter substrate. The amount of deposited soot is proportional to the time. Sooner or later, a thick soot layer is formed at the upstream side of the filter, and the filter is clogged. Resultantly, the filter backpressure is steeply increased.
2. In the case of the catalyzed filter, since the soot oxidation rate is extremely high, the soot deposited inside the filter is immediately oxidized. In this state, a soot layer is not thickened, and the increase in filter backpressure is prevented; i.e., the continuous regeneration is realized.
3. The catalyst coating area was changed. Three cases were considered: 1/3 upstream side in case 3A, 1/3 middle side in case 3B, 1/3 downstream side in case 3C. The soot oxidation is largely promoted only in the region of catalyzed area, but the amount of deposited soot in case 3A is smaller than those in cases 3B and 3C. This could be due to the fact that more soot accumulation is observed at the upstream area of the

filter.

4. The value of the filter backpressure in case 3A was almost equal to that in case 2 where the filter was entirely covered by the catalyst. This indicates that the catalyst coating at the upstream side is more effective, and the amount of catalysts could be reduced by 1/3 of the entire coating.

Acknowledgments

This work was partially supported by the Rare Metal Substitute Materials Development Project, New Energy and Industry Technology Development Organization (NEDO) in Japan.

References

[1] A. Yezerets, N.W. Currier, D.H. Kim, H.A. Eadler, W.S. Epling, C.H.F. Peden, Applied Catalysis B 61 (2005) 120.

[2] D. B. Kittelson, Journal of Aerosol Science 29 (1998) 575.

[3] I. M. Kennedy, Proc. Combust. Inst. 31 (2007) 2757.

[4] T. Tzamkiozis, L. Ntziachristos and Z. Samaras, Atmospheric Environment 44 (2010) 909.

[5] T. V. Johnson, SAE Technical Paper 2010-01-0301 (2010) 16.

[6] A. M. Stamatelos, Energy Conversion and Management, 38(1) (1997) 83.

[7] H. Yokota, S. Tahara, H. Ueno, K. Sakamoto, J. Aerosol Res., 18(3) (2003) 185.

[8] T. Tzamkiozis, L. Ntziachristos, Z. Samaras, Atmospheric Environment 44 (2010) 909.

[9] E. Wirojsakunchai, E. Schroeder, C. Kolodziej, D. E. Foster, N. Schmidt, T. Root, T. Kawai, T. Suga, T. Nevius, and T. Kusaka, SAE Technical Paper 2007-01-0320 (2007).

[10] K. Tsuneyoshi, O. Takagi, and K. Yamamoto, SAE Technical Paper 2011-01-0817 (2011) 297.

[11] G.C. Koltsakis, A.M. Stamatelos, Prog. Energy Combust. Sci. 23 (1997) 1.

[12] T. Nakajima, S. Sasaki, A. Kawai, K. Sakamoto, J. Aerosol Res., 15(4) (2000) 344.

[13] K. Yamamoto, M. Nakamura, H. Yane, and H. Yamashita, Catalysis Today 153 (2010) 118.

[14] K. Yamamoto, N. Takada, and M. Misawa, Proc. Combust. Inst. 30 (2005) 1509.

[15] K. Yamamoto, S. Oohori, H. Yamashita, S. Daido, Proc. Combust. Inst. 32 (2009) 1965.

[16] K. Yamamoto, S. Satake, H. Yamashita, N. Takada, M. Misawa, the European Physical Journal 171 (2009) 205.

[17] K. Yamamoto, K. Yamauchi, N. Takada, M. Misawa, H. Furutani, O. Shinozaki, Philosophical Transactions A, The Royal Society, London 369 (2011) 2584.

[18] S. Chen, and G. D. Doolen, Annual Reviews of Fluid Mech. 30 (1998) 329.

[19] Q. Zou, and X. He, Physics of Fluids 9 (1997) 1591.

[20] K. Yamamoto, He, X. and G. D. Doolen, Journal of Statistical Physics 107 (2002) 367.

[21] K. B. Lee , M. W. Thring, and J. M. Beer, Combust. Flame 6 (1962) 137.

[22] J. Song, M. Alam, A. L. Boehman, and U. Kim, Combust. Flame 146 (2006) 589.

[23] K. C. Oh, H. D. Shin, Fuel 85 (2006) 615.

[24] B. Chopard, A. Masselot, and A. Dupuis, Computer Physics Communications 129 (2000) 167.

[25] K. Yamamoto, Communications in Computational Physics, 13 (3) (2013) 769.

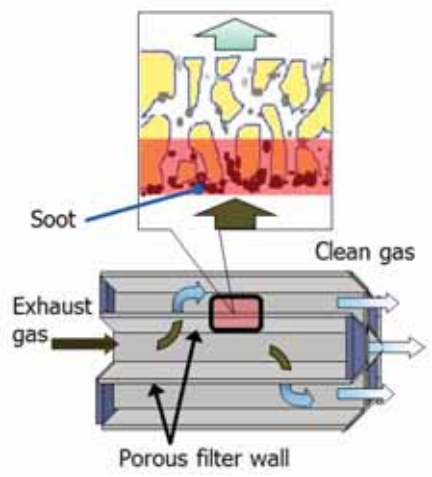

Fig. 1 A schematic of diesel particulate filter is shown. Upper figure shows PM trap inside porous filter wall.

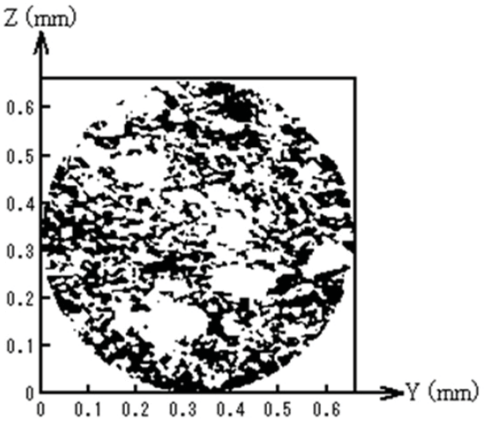

Fig. 2 DPF structure in *yz* plane of the DPF cross section at the center.

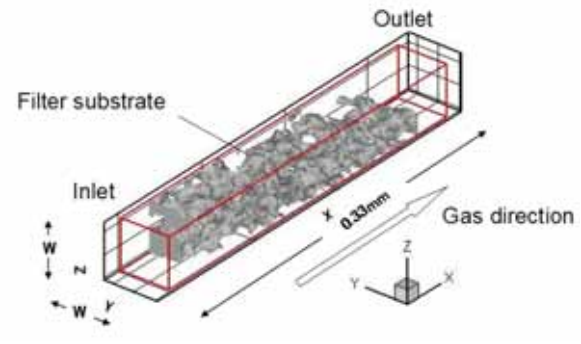

Fig. 3 Coordinate and numerical domain are shown. Exhaust gas passes through the filter in *x* direction. A part of CT data was inserted in the numerical domain for tomography-assisted simulation. The width of the numerical domain is *W*.

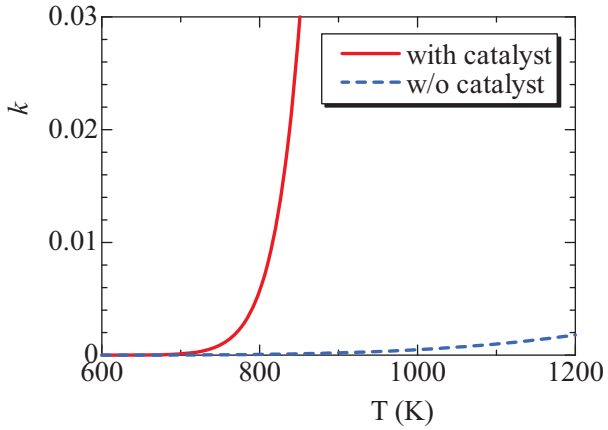

Fig. 4 Reaction rate constants with and without catalysts.

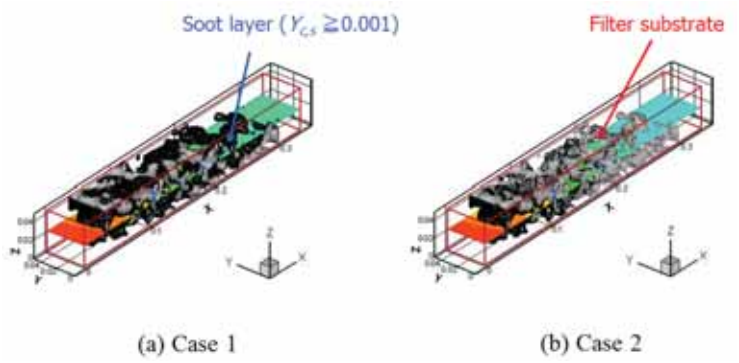

Fig. 5 Soot region of (a) without catalyst in case 1 and (b) with catalyst in case 2.

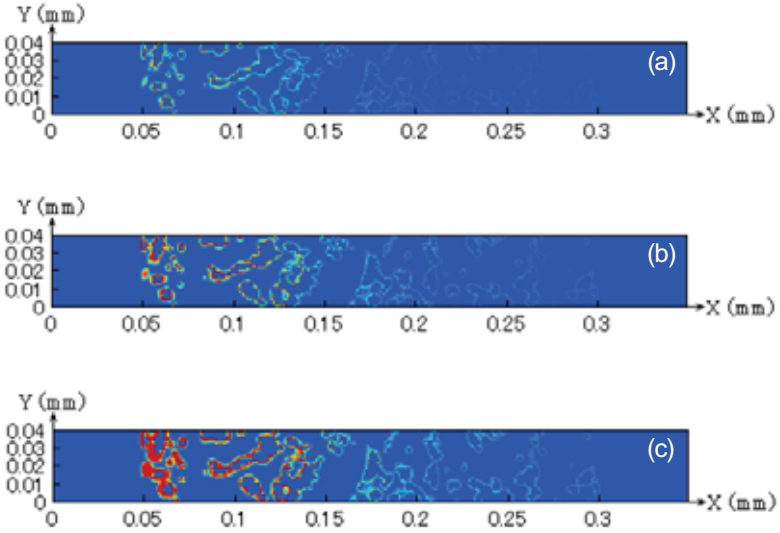

Fig. 6 Time-variation of soot deposition region in case 1 at (a) $t = 40$ s, (b) 80 s, (c) 120 s.

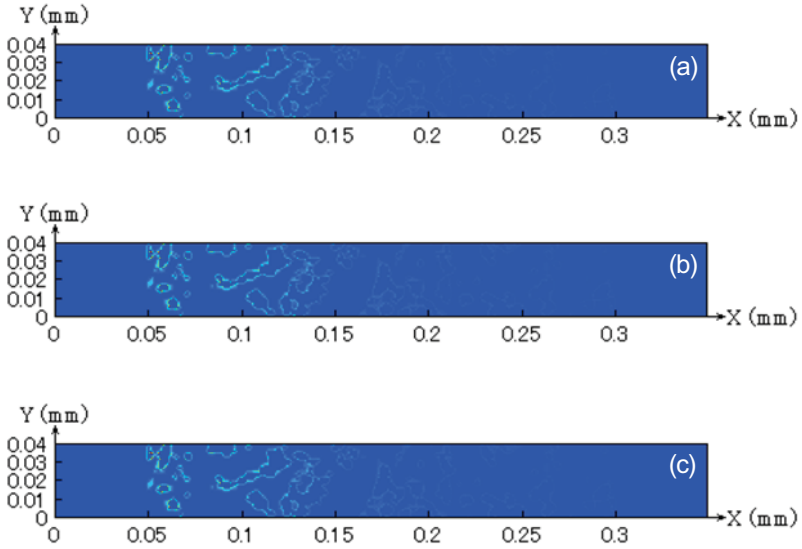

Fig. 7 Time-variation of soot deposition region in case 2 at (a) t = 40 s, (b) 80 s, (c) 120 s.

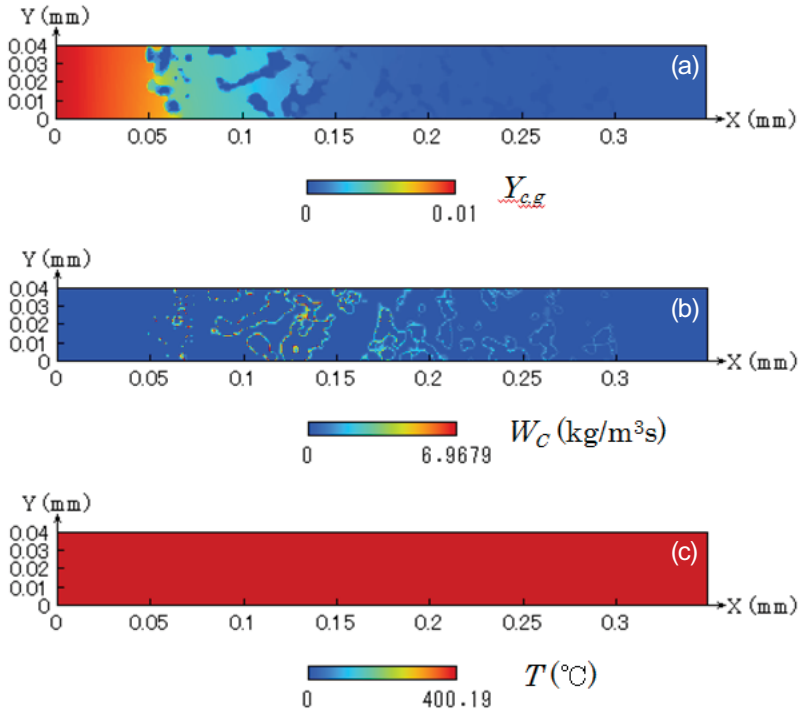

Fig. 8 Combustion field at t = 120 s in case 1; (a) soot in gas phase in upper figure, (b) reaction rate in middle figure, (c) temperature in lower figure.

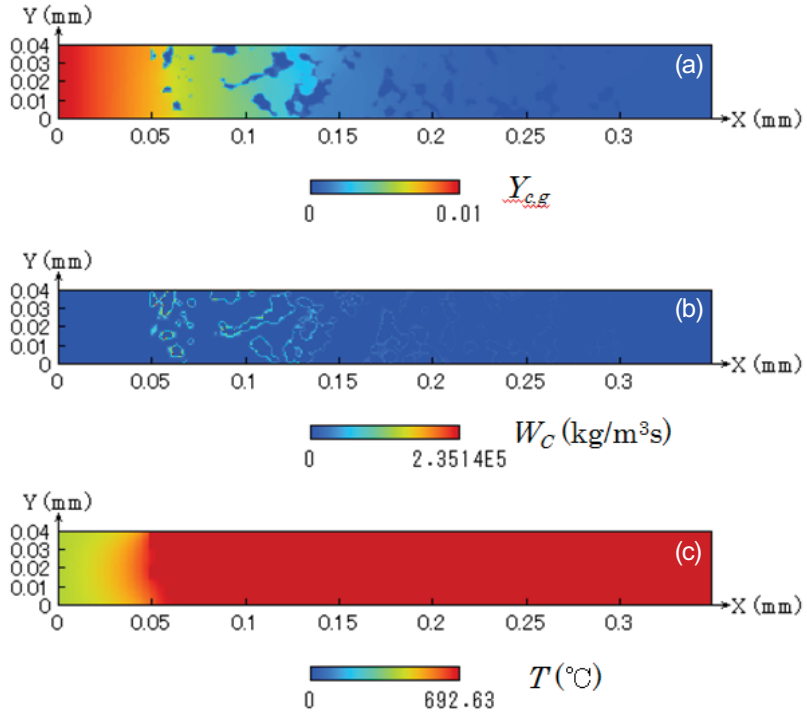

Fig. 9 Combustion field at t = 120 s in case 2; (a) soot in gas phase in upper figure, (b) reaction rate in middle figure, (c) temperature in lower figure.

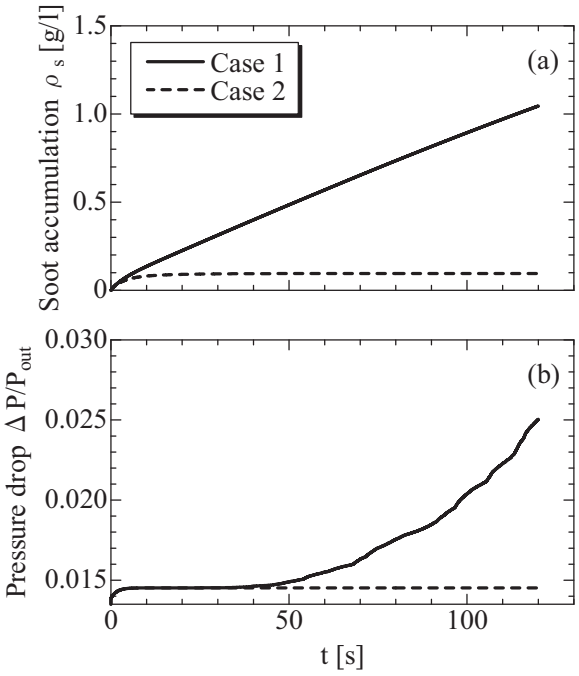

Fig.10 Profiles of (a) amount of deposited soot, (b) filter backpressure.

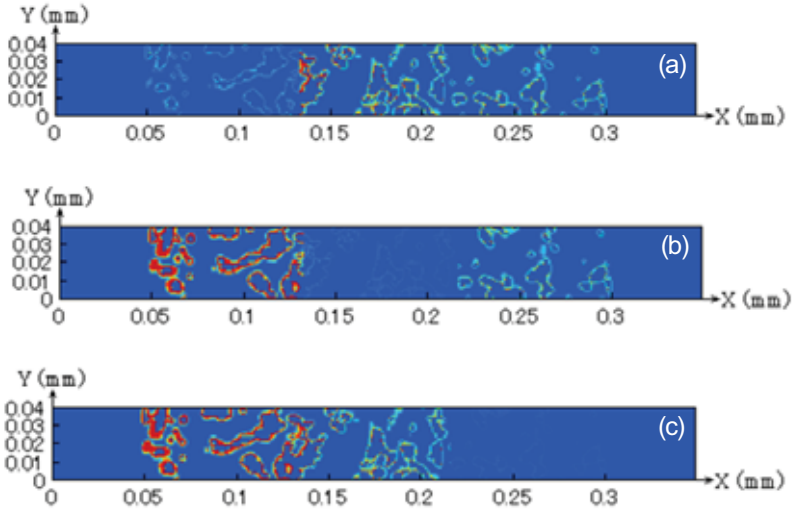

Fig. 11 Soot deposition region at t = 120 s in (a) case 3A, (b) 3B, (c) 3C.

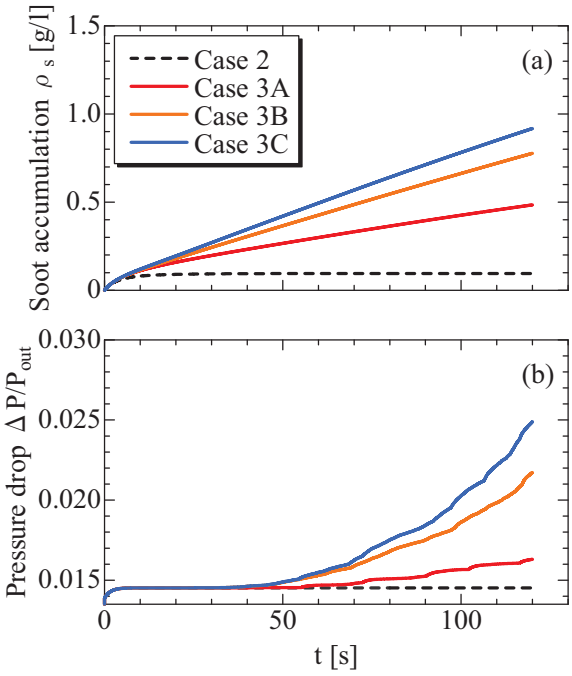

Fig.12 Profiles of (a) amount of deposited soot, (b) filter backpressure.

Table 1 Five cases with different catalyst-coating.

Case	Upstream	Middle	Downstream
1	No	No	No
2	Catalyzed	Catalyzed	Catalyzed
3A	Catalyzed	No	No
3B	No	Catalyzed	No
3C	No	No	Catalyzed

Table 2 Engine specifications

Model	NISSAN YD252
Engine Type	Inline 4 cylinder, DOHC
Cylinder head port	Tandem port
Displacement	2488 cc
Maximum power	126 kW @ 4000 rpm
Maximum Torque	403 Nm @ 2000 rpm
EGR System	EGR cooler
Turbocharger	Variable Geometry Turbo with mechanical control